Structural and sorption properties of bio-nanocomposite films based on κ-carrageenan and cellulose nanocrystals

Maria-Cristina Popescu[1*], Bianca-Ioana Dogaru[1], Dongyang Sun[2], Elena Stoleru[1], Bogdan C. Simionescu[1]

[1]*Petru Poni Institute of Macromolecular Chemistry of the Romanian Academy, Iasi, Romania*

[2]*School of Engineering and the Built Environment, Edinburgh Napier University, Edinburgh, UK*

Abstract

There is an increased interest on changing the synthetic based materials to biodegradable ones, especially with natural polymers, polysaccharides or proteins. In this research we prepared bio-nanocomposite formulations with different component concentrations and investigated their structural features, with focus on the interactions, sorption properties, and how the combination between them influences these properties. By infrared spectroscopy, principal component analysis (PCA) and two-dimensional correlation spectroscopy (2DCOS) was identified that in the blending process are involved the $-SO_4$ and C(4)-O-S groups of β-d-galactose, C–O groups, (O=S=O) of carrageenan and –OH and C–O groups from CNCs.

The water uptake and water sorption properties decrease with increasing the CNCs content in the formulations from about 15 % for κ to 10% for κC15 and from about 128 % for κ to 115 % for κC15, respectively. The increase of the CNCs content induced an increase of the water contact angle from 47° for κ to 90° for κC15, indicating once again the involvement of the free hydroxyl groups in the hydrogen bonded interactions.

[*] Maria-Cristina Popescu, *Petru Poni Institute of Macromolecular Chemistry of the Romanian Academy, 41A Gr. Ghica Voda Alley, Ro.700487, Iasi, Romania*, Phone: 0040 232 217454, Fax: 0040 232 211299, e-mail: cpopescu@icmpp.ro

Keywords: nanocomposite films; κ-carrageenan; cellulose nanocrystals; interactions; sorption properties

1. Introduction

Concerns about environmental impact and exhausting natural resources caused by non-biodegradable, petrochemical-based plastic packaging has raised interest in the use of biodegradable alternatives originating from renewable sources [1]. Due to environmentally friendly, nontoxic nature, and abundancy, the interest in the study of biodegradable natural polymer films has witnessed a steady increase, as well as their potential application range [2]. Furthermore, it could overcome the main shortcoming of synthetic polymers, which are mostly soluble in organic solvents. In the recent years, extensive investigation into biodegradable films prepared from various protein, polysaccharide and lipid-based biopolymer materials have been conducted [3, 4], biodegradable biopolymer attracting more attention as representative water-soluble polysaccharide in many research fields [5].

Generally, polysaccharide and protein film materials are characterized by high moisture permeability, low oxygen and lipid permeability at lower relative humidity, and compromised barrier and mechanical properties at high relative humidity [6]. Nonconventional sources of carbohydrates have been extensively studied. There are various unique carbohydrates that are found in marine organisms that represent a largely unexplored source of valuable materials. These nonconventional and underexploited renewable materials can be used as an interesting alternative to produce edible films and coatings [7].

κ-carrageenan (κ) is an interesting biopolymer extracted from certain species of red seaweed and composed of a linear chain of sulfated galactans [8]. It has good potential for development, because present good transparency, good tensile strength, gelling ability and good

film forming properties [9], but it has some limitation like poor barrier properties, and lower elongation [10]. The use of carrageenan as edible films and coatings already covers various fields of the food industry, such as application on fresh and frozen meat, poultry, and fish in order to prevent superficial dehydration [11], ham or sausage casings, dry solids foods, and oily foods [12], but also cosmetics and pharmaceuticals [13]. Even though κ is used in many applications, it forms films which do not present good mechanical and water-vapor barrier properties. Thus, further improvement is needed to increase their physical and mechanical properties [3]. Recently, special attention has been focused on the use of nanosized reinforcing agents into polymer matrix to form nanocomposite materials [14, 15]. The incorporation of well-dispersed nanofillers into a polymeric matrix may cause improved physico-chemical (such as mechanical, optical, thermal and barrier) properties of the polymeric matrix. Thus, Wahab and Abd Razak [16] reported that the incorporation of 3 wt% of halloysite clay nanotubes into the κ-carrageenan matrix improved the mechanical, bioactivity and model drug release properties of the films. Also, the incorporation of metallic nanoparticle like ZnO and CuO improved the swelling ratio of carrageenan films and exhibited higher mechanical properties, thermal stability and UV-screening [17]. The incorporation of 5 wt % SiO_2 nanofiller increased significantly the tensile strength of nanocomposite films and decreased the moisture uptake and oxygen transmission rate [18].

In the last years the incorporation of cellulose nanocrystals in different polymetric matrices was reported. Cellulose nanocrystals (CNCs) are increasingly used as load-bearing constituents in developing new biodegradable materials due to their high aspect ratio, good mechanical properties, and fully degradable and renewable character [19]. As compared to other inorganic reinforcing fillers, CNCs have many additional advantages, including a positive ecological footprint, wide variety of fillers available throughout the world, low density, low

energy consumption in manufacturing, ease of recycling by combustion, high sound attenuation, and comparatively easy processability due to their nonabrasive nature [5-7]. Few recent papers reported the utilization of small amounts of CNCs (1-9 wt%) in order to improve the properties of κ-carrageenan films [20-22]. It was observed that the incorporation of 3% CNCs in κ-carrageenan matrix present the best enhancement of oxygen barrier properties of polymeric matrix and the tensile strength and modulus increased from 45.7 MPa to 710 MPa at 5 wt% CNCs [20]. Similar results are also reported by the others research groups [21, 22].

The properties of the nanocomposite materials are strongly dependent of the amount of the nanofiller and crosslinker, but also on the preparation conditions. Therefore, in this study 5, 10 and 15 wt% of CNCs and glycerol were used to prepare bio-nanocomposite films through solution casting method. In order to be used as coating materials, the structural and sorption properties were evaluated.

2. Materials and methods

2.1. Materials and preparation of the films

κ-carrageenan (κ) and glycerol (>99.5%) were purchased from Sigma Aldrich (Sigma Aldrich, St. Louis, MO, USA). Cellulose nanocrystals (CNCs) (sulfur content: 91 mmol kg^{-1}, Zeta-potential: −28.5 mV) was produced from cellulose pulp by sulfuric acid hydrolysis, and kindly supplied by Melodea Ltd. (Rehovot, Israel). TEM images of the aqueous CNC suspension revealed rod-like particles (length: 20–500 nm [mean 170 nm]; width: 2–20 nm [mean 6.8 nm]). [23].

The solution of 3wt% κ-carrageenan was prepared by the solubilization of the solid particles in distilled water at 60 ^{o}C and 1200 rpm for 1h.

The nanocomposite formulations were obtained by mixing the previous prepared solution with cellulose nanocrystals (CNCs) suspension in different proportions in order to achieve final concentrations of 95 wt% κ /5 wt% CNC, 90 wt% κ /10 wt% CNC, 85 wt% κ /15 wt% CNC and with 0.05 mL of glycerol (concentration of 30% based on κ-carrageenan powder weight w/w). To ensure a good homogeneity, all formulations were mechanically stirred on a heating plate for 30 min, at 60 ^{o}C and 1000 rpm, followed by high speed stirring for other 5 min by using an ultraturax. Previously prepared solutions were transferred in glass Petri dishes and kept in an oven at 45 ^{o}C for 24h. Resulted films presented a thickness of 0.15±0.01mm (the presented value is an average of five measurements taken in five random points for each sample). The composition and samples code are presented in Table 1.

Table 1. The composition and sample code for the studied samples

Sample code	κ-Carrageenan (wt%)	CNC (wt%)
κ	100	-
C	-	100
κC5	95	5
κC10	90	10
κC15	85	15

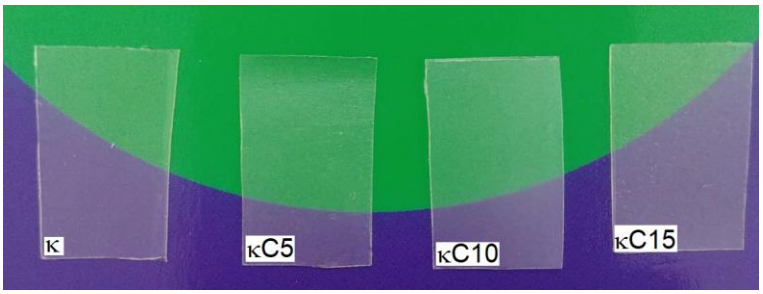

Fig.1 Visual aspect of κ and κC films

From Fig. 1 can be observed that κ and κC films are transparent, and the transparency was not diminished after the CNC addition.

2.2. Methods

2.2.1. The *ATR-FT-IR spectra* of the films were measured at 4 cm^{-1} resolution on a Bruker ALPHA FT-IR spectrometer using a Diamond crystal. Five recordings were performed for each sample, the evaluations being made on the average spectrum obtained from these recordings.

Two-dimensional correlation spectroscopy (2D-COS). The synchronous and asynchronous 2DCOS spectra was constructed using Shige program.

2.2.2. Wide Angle X Ray Diffraction – WAXD was performed on a Diffractometer D8 ADVANCE (Bruker AXS, Germany), using the CuKα radiation (λ=0.1541 nm). The working conditions were 40 kV and 30 mA, 2s/step, and 0.02 degree/step. All diffractograms were recorded in the range 10-90 2θ degrees, at room temperature.

2.2.3. Scanning electron microscope (SEM) - Film samples were investigated using a scanning electron microscope (SEM) (S4800 field emission SEM, Hitachi, UK). Each film was attached to SEM aluminium stub before being gold coated for 90 seconds using a sputter coater (EMITECH K550X, Quorumtech, UK). During imaging, 3kV and 8.5 mm were used as the acceleration voltage and observation distance, respectively.

2.2.4. Water vapour sorption measurements. For the adsorption/desorption tests, two replicates with a surface area of 1 cm^2 were used for each sample. Prior the test, the samples were maintained in an oven for 24h at 65 ^oC until constant weight was reached. The samples were then exposed in sealed containers presenting different relative humidity values, reached by saturated salt solutions, selected to cover the entire RH range of the isotherm having theoretic values of

8.5%, 11.3 %, 17.7%, 22.5 %, 32.8 %, 43.2 %, 54%, 57.1 %, 68.9 %, 74%, 78%, 81%, 85%, 93.6 % and 99 %, respectively, at 25 ^{o}C. To record the exact RH values, each container has been equipped with a LogTag thermo hygrometer. The samples were maintained at 25 ^{o}C for a period of 48h in a specific container at lower RH values and for a period of 24 h in a specific container presenting higher RH values and then they were weighed and transferred to the next medium with higher RH values for the adsorption measurements, and vice versa for desorption measurements.

2.2.5. Water uptake test. Oven dried samples with a constant dry mass were placed in a desiccator at 57% RH (using $Mg(NO_3)_2$ saturated solution). The samples were removed from the medium and weighed periodically until a constant mass was observed.

2.2.6. Determination of swelling degree. Samples (two replicates for each film) with dimensions of 1 cm^2 were maintained in an oven at 65°C for 24 h until constant mass was reached and then they were placed in distilled water at 25 °C and weighted periodically every 5 min up to 45 min, and then every 15 min up to 4h. After that the films were removed from the water and placed back in the oven at 45°C for 24 h, until they reached a constant weight to obtain the final dry mass of the films.

The moisture content (MC%), water uptake (WU%) and percentage of absorbed water (M%) were calculated by using the same type of equation:

$$MC\%(WU\%)(M\%) = \frac{M_f - M_i}{M_i} x100$$

where: M_f is the mass of the sample recorded at a certain RH value or at a time t, and M_i is the dry mass of the sample.

2.2.7. Dry-in time of water droplets on the surfaces and absorption - the ability of water-uptake and dry-in time of a water droplet was evaluated by placing three droplets with comparable size with a syringe on each of the chosen surfaces. The water was colored with a

natural extract of red beet to make it visible. The time until the droplets were dry (dry-in time) was measured and the removability of the dried droplets was evaluated by identifying the absorption into the surface.

2.2.8. Contact angle measurements. The static contact angles for the polymer films were determined by the sessile drop method, at room temperature and controlled humidity, within 30 s (the time corresponding to a metastable equilibrium between the liquid droplet and the tested surfaces) using a CAM-200 instrument from KSV, Finland. The measurements were performed using 1 μL drop of water on the film surface. Contact angle measurements were taken on five different locations on the surface and the average values were further considered. All measurements were done on the side of the films in contact with the air during drying.

3. Results and discussion

3.1. FT-IR spectroscopy

IR spectroscopy is a powerful method to evaluate the structure of the components and the interaction between them. κ-carrageenan is a linear polysaccharide consisting of alternating 3-linked-β-D-galactopyranose and 4-linked-α-D-galactopyranose units, while the cellulose structure shows the β-(1→4)-D-glucopyranose repeat units [8]. Since the basic structures of both polysaccharides are composed of glucopyranose repeating units, the IR spectra have some similarities. Fig. 2 present the IR spectra of the components and the blends.

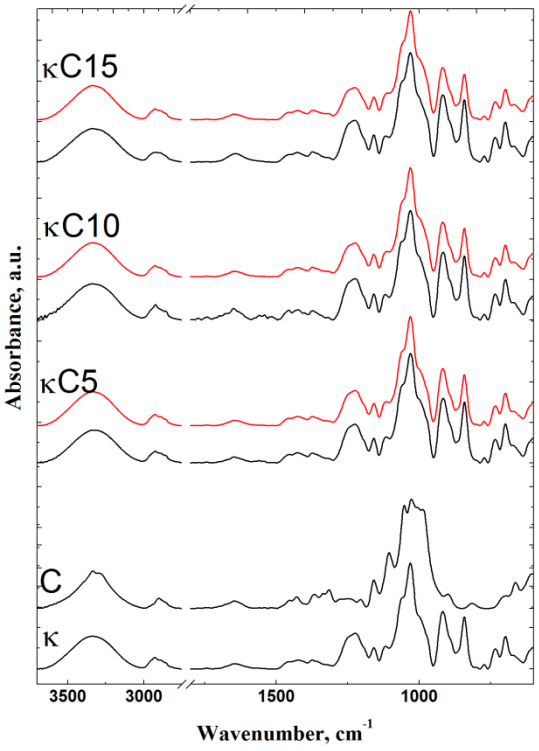

Fig. 2. FT-IR spectra of pure components and blends

As can be seen from Fig. 2, both components present a broad band in the spectral region between 3700-3000 cm^{-1} assigned to stretching vibration of OH groups and 3 bands in the 3000-2700 cm^{-1} spectral region assigned to symmetric and asymmetric stretching vibration of CH_3 and CH_2 groups [24].

In the fingerprint region (1800-600 cm^{-1}) IR spectra of κ-carrageenan shows spectral bands at 1639 cm^{-1} assigned to deformation vibration of OH groups of absorbed water, 1457, 1425 and 1225 cm^{-1} assigned to in-plane deformation vibration of OH and H–O–C groups, at 1367 cm^{-1} assigned to in-plane deformation vibration of CH groups, at 1323 cm^{-1} assigned to rocking vibration of CH_2 groups, at 1246 cm^{-1} assigned to asymmetric stretching vibration of S=O groups, at 1194 cm^{-1} assigned to symmetric stretching vibration of S=O groups, at 1161 cm^{-1} asymmetric stretching vibration of C–O–C groups, 1113 and 1034 cm^{-1} assigned to stretching

vibration of C–O groups and 916 cm^{-1} assigned to stretching vibration of 3,6-anhydrogalactose (C–O–C) and 843 cm^{-1} assigned to stretching vibration of C_4-O-S standing for total $-SO_4$ and C_4-O-S of β-d-galactose [24, 25, 26]. IR spectra of CNC present characteristic bands at 1638, 1457, 1357 and 1235 cm^{-1} assigned to stretching and in plane deformation vibration of OH groups; at 2940, 2898, 1372, 1282 and 1317 cm^{-1} assigned to stretching, deformation and rocking vibration of CH groups; at 1204, 1163 and 1060 cm^{-1} assigned to stretching and deformation vibration of C–O–C groups from pyranose ring and 897 cm^{-1} assigned to stretching vibration of ring [27, 28].

Due to the similarities between the components and because the amount of CNCs in the blends is relatively small the IR spectra of the nanocomposite films are very similarly with the κ spectrum. In order to evidence the small differences appeared in these spectra, the experimental spectra were compared with the calculated ones (using the components spectra and the additivity low). Since neither this method could evaluate the interactions between the components of the mixtures more sensitive methods such as PCA and 2DCOS were used.

Principal component analysis (PCA) is used to visualize interrelationships among the independent variables and is useful in identifying data outliers, and to investigate the difference between spectra and derive parameters characterizing the interaction between the different components. The principal component factor 1 (PC1) describes 91%, principal component factor 2 (PC2) describe 7% and principal component factor 3 (PC3) describe 1 % of data the variance, so 99% of the existed variances in the studied spectra is captured using these three dimensions instead of the initial data. The three-dimensional coordinate system of the PC scores is plotted in Fig. 3.

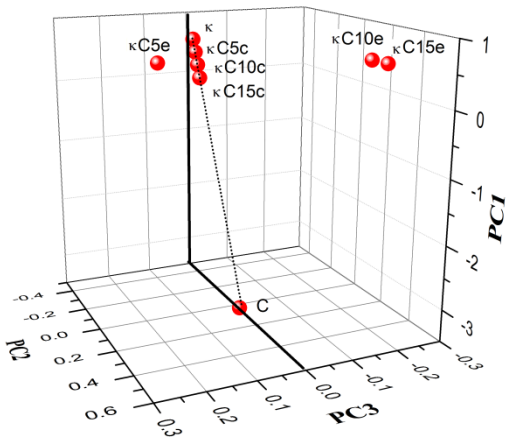

Fig. 3. Three dimensional PCA score plots of the studied samples

It can be observed that the calculated spectra appear in the same plane (PC1-PC2 plane) with the components, the position depending on the component's composition. Therefore, this plane can be defined as the non-interaction reference plane. In this case the variation on PC3 direction is about zero. In case of experimental samples, a significant variation on PC3 score direction can be evidenced. Thus, the plane PC2-PC3 can be defined as the interaction plane. The distances between the experimental spectra and the calculated spectra are evidenced in case of all studied samples, this indicating the presence of the interactions.

2D IR correlation spectroscopy (2DCOS) is powerful in analyzing the rather complicated IR region, and may be able to identify spectral signatures of the specific interaction in polymer blends. The 2D study of the κ/CNCs blends was raised in order to discriminate the bands of the components from the highly overlapped complex spectra and also to evaluate the intermolecular interaction between the components. For this, the 2D spectra constructed from the experimental and calculated blend spectra were compared. In the case of immiscible blends the synchronous 2D correlation maps can be calculated, but not their asynchronous counterparts. This is because, in principle, there should be little or no interaction between the blend components and the

intensities of all the bands in the spectra should change linearly with concentration [29]. In the case of miscible blends, the small frequency or band width shifts have a pronounced effect on the 2D correlation spectra. In our study both synchronous and asynchronous spectra were obtained and the existence of inter-molecular interaction between blend components was observed.

To keep the discussion simple, the 2D correlation spectra were constructed for two spectral regions 3700-2700cm^{-1} and 1400–700cm^{-1} from both calculated and experimental data.

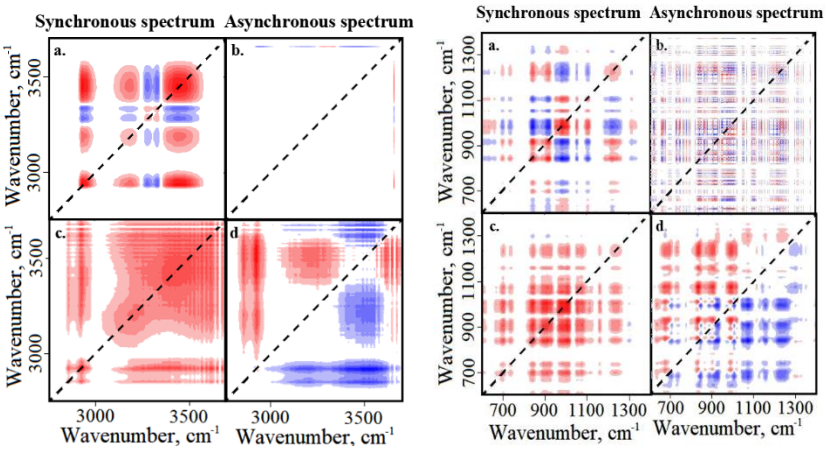

Fig. 4. 2DCOS spectra for calculated (a, b) and experimental (c, d) data in the 3700-2700 cm^{-1} and 1400-600 cm^{-1} spectral regions

The synchronous spectrum in the 3700-2700 cm^{-1} region of calculated data shows auto-peaks at 3447, 3335, 3295, 3170 and 2940 cm^{-1}, four positive cross-peaks at 3335 vs. 3295 cm^{-1}, 3447 vs. 3170 cm^{-1}, 3447 vs. 2940 cm^{-1} and 3170 vs. 28940 cm^{-1} and six negative cross-peaks at 3447 vs. 3335 cm^{-1}, 3447 vs. 3295 cm^{-1}, 3335 vs. 3170 cm^{-1}, 3295 vs. 3170 cm^{-1}, 3335 vs. 2940 cm^{-1} and 3295 vs. 2940 cm^{-1}. The positive cross-peaks indicate that the two spectral variables increase or decrease together, and the negative cross-peaks depict that one of the spectral intensities is increasing while the other is decreasing [30]. The band located at 3295 cm^{-1} is

assigned to the stretching vibration of OH groups from CNCs. That means that the band located at 3335 cm^{-1} is also assigned to CNCs, while those located at 3447, 3170 and 2940 cm^{-1} are characteristic bands of κ.

In the case of experimental spectra, the synchronous spectrum in this region consist in two large superposed auto-peaks at 3421 and 3248 cm^{-1} and two small auto-peaks at 2921 and 2851 cm^{-1}. All bands form positive cross peaks indicating that all these bands vary in the same direction. The bands at 2921 and 2851 cm^{-1} are characteristic to stretching vibration of CH groups from κ, thus, the bands at 3421 and 3248 cm^{-1} correspond to κ too. In the case of experimental data, the asynchronous spectrum present clear bands, which indicate specific interactions and/or conformational rearrangements. It is also known that asynchronous spectrum has the deconvolution capacity. In this region, new bands are evidenced at 3517 and 3194 cm^{-1} and can be considered as interaction band. The band at 3517 cm^{-1} was assigned to multiple formation of an intermolecular hydrogen bond between phenolic groups and their combinations with alcoholic groups and the band at 3194 cm^{-1} stretching vibration of O6-H6···O3 intermolecular in cellulose [31].

In the 1400-600 cm^{-1} region the synchronous spectrum of calculated date present 8 auto-peaks at 1224, 1104, 1055, 985, 915, 845, 739 and 701 cm^{-1}. These bands form between them a great number of positive and negative cross-peaks. Analyzing the sign of the cross-peaks, the bands assigned to κ and CNCs can be discriminated. Taking into account the assignments and the sign of the cross-peaks, the bands from 1224, 919 and 845 cm^{-1} are characteristic bands of κ, while the bands from 1315, 1104, 1055 and 985 cm^{-1} are characteristic to CNCs. In case of experimental data synchronous spectrum show 10 auto-peaks at 1234, 1160, 1067, 1051, 1006, 975, 911, 841, 737 and 699 cm^{-1}. Comparing with synchronous spectrum for calculated data, in this case appear 3 new auto peaks at 1160, 1067 and 1006 cm^{-1} and the auto peak at 1224 cm^{-1} is

shifted to higher wavenumber. These indicate the involvement of C-O groups of the components in the blend formation. Taking into account the synchronous and asynchronous cross-peaks and using the Noda's rule, the following sequence of band variation was obtained:

$$841\ cm^{-1} > 1006,\ 1067 cm^{-1} > 1234\ cm^{-1} > 1160\ cm^{-1}$$

indicating that, in the blending process, the first are changing the band assigned to stretching vibration of C(4)-O-S standing for total $-SO_4$ and C(4)-O-S of β-d-galactose, followed by the bands assigned to stretching vibration of C–O groups, the bands assigned to symmetric vibration of sulfate ester (O=S=O) and/or bending vibration of OH groups and symmetric stretching vibration of C–O groups from pyranose ring and the bands assigned to asymmetric stretching vibration of C–O–C groups.

3.2. X-Ray diffraction (XRD)

The polysaccharides present physical interactions (like hydrogen bonding between the molecular chains and also with water) having a great impact on their molecular mobility and functional properties. In order to evaluate the degree of crystallinity of the studied films, their X-ray diffractograms (see Fig. 5) were recorded.

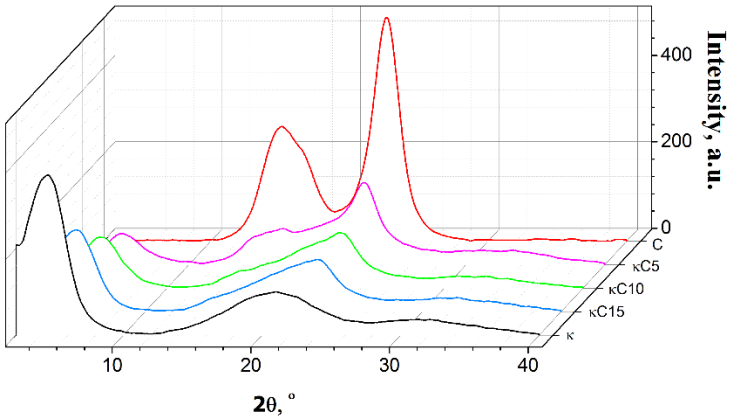

Fig. 5. XRD pattern of the components and blends

In the case of κ, tree signals were observed at 4.54, 21.11 and 31.76º. The addition of nanoscale particles can change the crystallization kinetics, crystalline morphology, crystal forms, and crystallite size [32]. These changes can significantly affect the mechanical and physical properties of the composite materials. The CNC diffractogram present the specific signals assigned to cellulose, namely: 15.1º assigned to the (101) plane, 16.4º assigned to the $(10\bar{1})$ plane and the 22.7º assigned to the (200) plane of cellulose I [31]. In the case of blends the diffraction signals for both κ and CNC are sifted to higher value with increasing the CNC content, thus the signal from 4.5º is shifted to 5.3º, 15.1º at 15.5º, 16.4º at 16.7º, 21.1º is combined with that from 22.7º of CNC and is shifted at 22.6º and the signal at 31.7º at 31.3º. These shifting induce an increasing in the lattice distance with increasing the CNC content. The incorporation of the rigid molecules of CNC in the κ matrix induces an orientation of the polymeric molecules and favour the formation of hydrogen bonds between the polymeric chains.

3.3. Scanning electron microscope (SEM)

In Fig. 6 are presented the scanning electron microscopy (SEM) images of the κ and κC nanocomposite films.

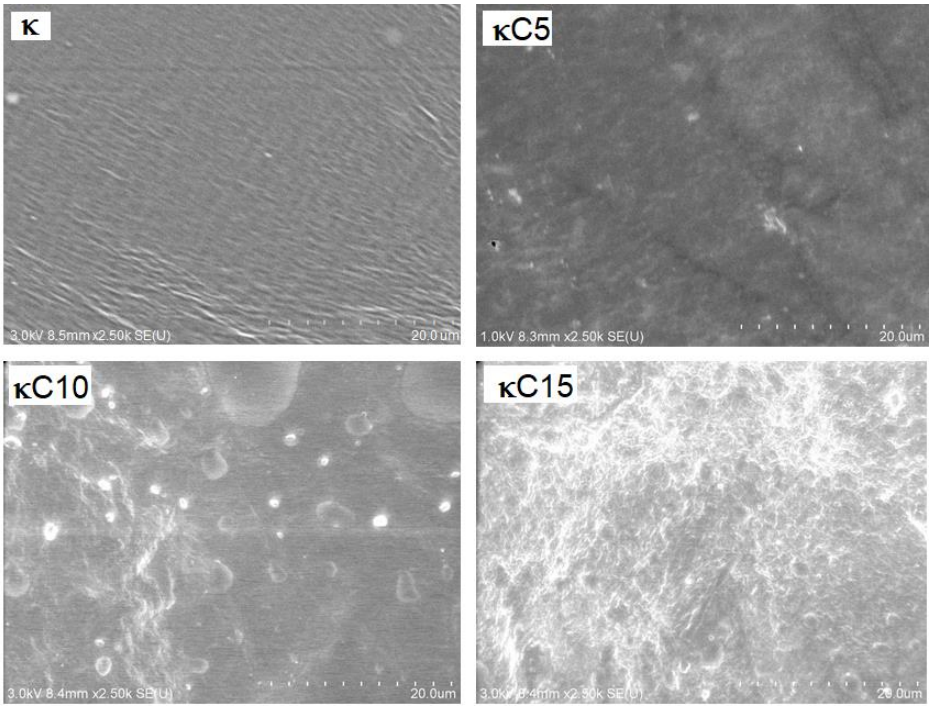

Fig. 6. Morphological aspect of κ and κC nanocomposite films

The surface of the κ-carrageenan film shows a uniform and smooth surface, but by addition of the CNCs into the polymeric matrix the films surface become less homogeneous and the CNCs are observed to be well dispersed. The images also showed a good adesion between the polymeric matrix and the filler, which may be due to the presence of a high number of hydrogen bonds between the formulation components.

3.4. Water sorption properties

Water sorption can induce physical changes in the polymeric structure of materials and the structure of sorbed water into these materials reflects their physical and chemical properties [33]. Hydrophilic polymeric materials adsorb and/or desorb water molecules from / into the surrounding environment, tending to reach equilibrium when the environmental RH is stable [34, 35]. In this context, the sorption properties of such materials represent a decisive factor for

further development of the polymeric materials with special properties, their application domain, long-term performance or service life. Therefore, in order to modify / improve the sorption properties of hydrophilic polymers like κ-carrageenan, the addition of nanofillers or crosslinking (plasticizing) agents is important [36, 37].

Water adsorption is a process in which the water molecules penetrate the polymeric matrix via physical adsorption, chemisorption and condensation. The relationship between the moisture content (MC) and environmental RH is known as a sorption isotherm, which is also strongly dependent on the surrounding temperature [35, 36].

The sorption isotherms at different RH values for the studied films are presented in Fig. 7.

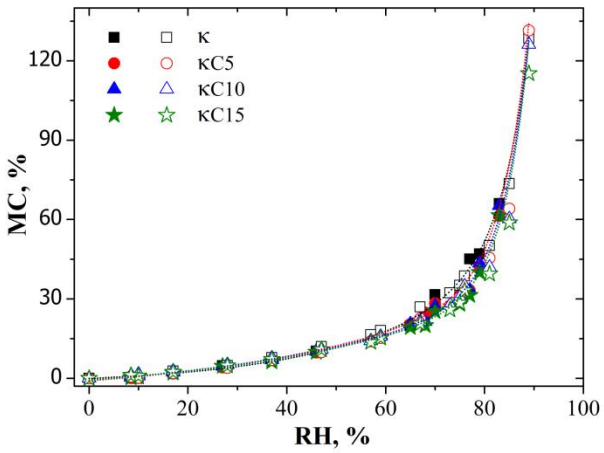

Fig. 7. Sorption isotherms for the studied films (full symbols represent the adsorption process, open symbols represent the desorption process)

The films adsorb small amount of water molecules at lower values of RH, followed by a gradual increase of the MC up to about 80 %RH, and exhibiting an asymptotic shape at the upper end of the curves. Up to about 50 %RH all the films represent about the same value of the MC%, after that, the κ film present the higher values, and with the increase of the CNCs content in the

films, the recorded MC% is lower. Exception is observed at maximum RH value (90%), where the highest value for the MC is recorded for the κC5 film (of 131%), while for κ was of 128%. This further decreases with the increase of CNCs content in the nanocomposite materials, being of 126% and 115% for the κC10 and κC15, respectively.

As mentioned before, the films were prepared by using κ-carrageenan, CNCs in various proportions, as well as glycerol as crosslinking agent. In order to observe only the influence of the CNCs on the polymeric matrix, we used glycerol also for the κ film. Balqis et al. [24] observed that the addition of the crosslinkers in κ-carrageenan induces a reduction in the MC, mentioning that this is due to "a complete reaction between small amounts of the plasticizer and the free sites of κ-carrageenan" [24]. The same effect was further induced by the addition of CNCs in the composition.

The obtained isotherms are represented by the IUPAC Type III pattern, which describe generally the adsorption of adsorbate on macro-porous adsorbents with weak adsorbate-adsorbent interactions. The adsorbate molecules clusters around the favorable sites on the surface of a non-porous or macro-porous solid [38]. It has been presented in literature [34, 35, 39] that the adsorbed water molecules are divided in several categories – single water molecules, aggregated water molecules and localized interactions of water molecules with other molecules or with the polymer – presenting distinct thermodynamic properties depending on the type of interaction, degree of interaction, as well as the polymeric structure. Further the localized interactions were subdivided in water molecules which are weakly bounded to the polymeric matrix or to other water molecules – so called freezing water, and water molecules strongly bound to polar groups in the polymeric matrix, so called non-freezing water.

In order to discriminate the different types of interactions between the water molecules and hydrophilic sites of the composite materials, the infrared spectra of the films were recorded.

When the water is adsorbed in the films, strong variation of the bands from 3750-3000 cm^{-1} region associated with stretching vibration of OH groups involved in hydrogen bonds and from the 1770-1504 cm^{-1} associated with deformation vibration modes was identified (spectra not shown). At the same time, with the increase of the moisture content in the films a shifting to higher wavenumber of the bands from 1033 cm^{-1} (to 1039 cm^{-1}), 3344 cm^{-1} (to 3365 cm^{-1}) in the case of κ spectrum, and from 1032 cm^{-1} (to 1040 cm^{-1}), and 3338 cm^{-1} (to 3352 cm^{-1}) in κC15 spectrum, and to a lower wavenumber of the band from 1644 cm^{-1} (to 1640 cm^{-1} – in κ spectrum and to 1639 cm^{-1} – in κC15 spectrum) was observed. The band from 1033 cm^{-1} is assigned to C-O-C stretching vibration while the other two bands are associated with the OH groups present in structure of both κ and CNC as well as in the structure of the crosslinking agent. The changes in both shifts of the maxima and intensities of these bands with increase of the MC% have been related to modifications in the molecular environment of the corresponding groups due to water-polymer interactions. It was indicated that the OH deformation vibration band "is featureless, with no evidence of underlying multicomponent structure" [40] but the OH stretching vibration band from 3361 cm^{-1} displays a complex profile with two observable maxima suggesting the presence of at least two different H-bond interactions, therefore further investigation was focus only on the 3750-3000 cm^{-1} region.

The difference spectra in the 3750 – 3000 cm^{-1} region for κC15 (as an example) obtained by subtraction of the dry film spectrum from the spectra presenting different MC contents, along with the second derivative spectra plotted in the same region are presented in Fig. 8.

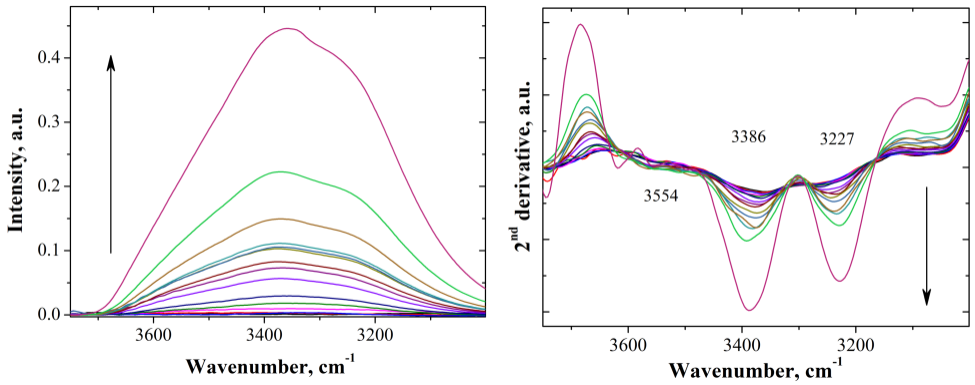

a. b.

Fig. 8. Difference spectra (a) and 2nd derivatives (b) of κC15 in the 3750-3000 cm^{-1} region

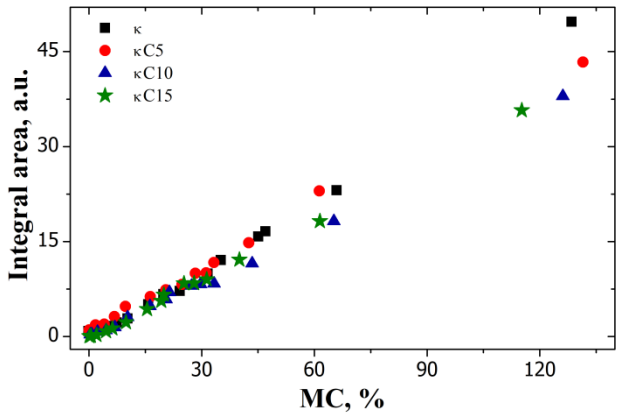

Fig. 9. Integral area of the band from 3750-3000 cm^{-1} versus moisture content for the studied samples

From Fig. 8a one can observe the increase of the integral area of the water band with the increase of the moisture content, as well as the presence of more than only one signal (maximum at 3361 cm^{-1} and a shoulder at about 3265 cm^{-1}). To identify the water dependence, the integral area was plotted against the MC% of the samples. As can be observed from Fig. 9, there is a linear dependence between them, decreasing with the increase of the CNC content in the samples. Further, from the second derivative spectra (Fig. 8b) was possible to evidence the presence of the

component bands at 3227, 3386 and 3554 cm^{-1} which form the water band envelope. According to Cotugno et al. [41] the adsorption process in polymers can be explained by an association model, where three different species of water can be spectroscopically distinguished, namely: S0 – related to asymmetric OH stretching of non-associated water, representing the water molecules which do not form any hydrogen bond with the polymer matrix; S1 – related to water molecules bonded to specific sites via weak hydrogen bond interactions and S2 – related to water molecules bonded to specific sites via strong hydrogen bond interactions. Therefore, S0 water molecules may be present in the pores or are molecularly dispersed with no H-bond interactions, S1 water molecules interact moderately forming water-polymer or water-water associations, while S2 water molecules are characterized by stronger H-bond interactions with low mobility [35, 41]. It is generally indicated that the high wavenumber OH stretching vibration band from 3554 cm^{-1} can be associated to S0 water molecules, 3386 cm^{-1} with S1 water molecules, while the low wavenumber of the OH stretching band from 3227 cm^{-1} can be assigned to water molecules strongly interacting with the polymer (S2 type).

The relative magnitude and the correlation between the bands can be observed in the 2D correlation spectra. In Fig. 10 synchronous and asynchronous spectra of κC15 sample are presented as an example (the other 2DCOS spectra present similar shapes).

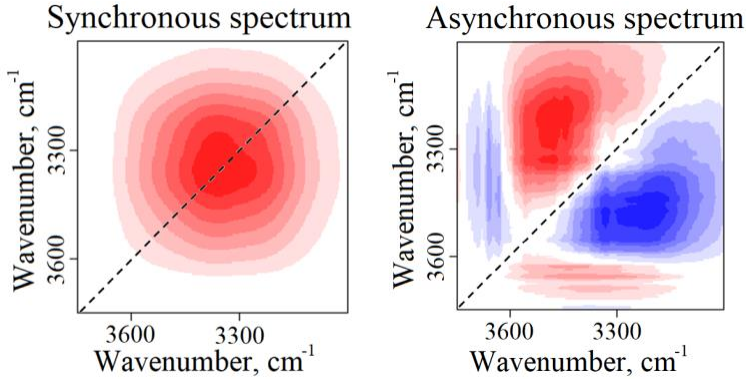

Fig. 10. 2DCOS synchronous (a) and asynchronous (b) spectra of water stretching band in the 3750-3000 cm^{-1} region for the κC15 sample

The synchronous spectra (Fig. 10a) present only one large auto-peak at 3367 cm^{-1} (the maximum vary in close limits between the samples), while the asynchronous spectra (Fig. 10b) indicate that the OH stretching band is separated in three components at 3605, 3438 and 3312 cm^{-1} representing the shifts of the bands from 3554, 3367 and 3227 cm^{-1} (as observed in second derivative spectra). The appearance of a peak in the synchronous spectrum is an indication of modifications in the corresponding band due to variations in the amount of moisture content, while the appearance of the peaks in the asynchronous spectra is regarded as a measure of dissimilarity of the spectral intensity variations [35].

The positive and negative correlation between the bands gives information regarding the sequential order of the intensity changes [30]. By applying Noda's rule, the following sequence of the band's variation: 3438 cm^{-1} > 3312 cm^{-1} > 3605 cm^{-1} was identified. This indicate that water molecules are linked to polymer hydrophilic sites via moderate H-bonds (S1 type) before forming stronger H-bonds with the matrix (S2 type) and diffuse into the free volume (S0 type) of the polymer matrix. The same behaviours have been identified by Jin et al [42] and Popescu et al [35].

3.5.Water uptake

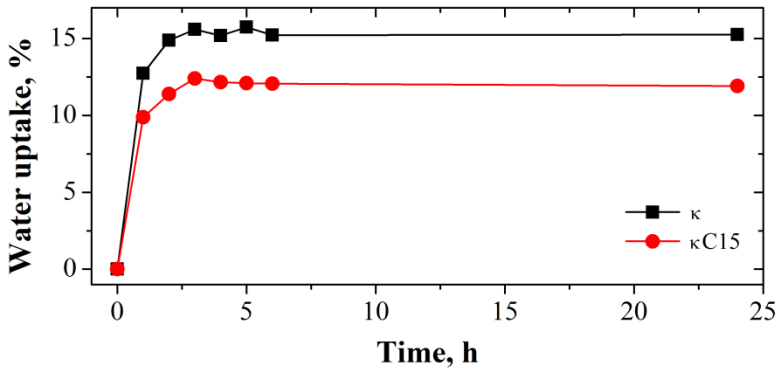

Fig. 11. Water uptake percentage of selected films after exposure at 57 %RH for 24h

The percentage of water uptake recorded for the κ and κC15 films for a period of 24h is presented in Fig. 11. The films reached the equilibrium in about 3h, after this time the values remaining constant. The highest amount of adsorbed water molecules of 15.2% was observed for κ film, while for the other one, κC15, the recorded value was of 11.9%. Similar values were observed by Balqis et al. for κ films crosslinked with glycerol (30%) [24].

3.6.Determination of swelling degree

Swelling properties of polymeric films are influenced by the addition of a nanofiller in the matrix as well as by the crosslinking agent. They show the stability of the materials in water, being an indication of long-term performance. The swelling behaviors of the films over a period of 120 min is presented in Fig. 12. The films presented similar behavior and reached the equilibrium rate after about 60 min, the highest values being observed for the κ film, followed by κC5 and κC10. κC 15 present almost the same behaviors as κC5 and κC10 up to about 30 min, then its swelling is reduced comparing to the other films. After 120 min it was observed a

decrease in the swelling values, indicating that might be a loss of the material in water after this time.

Farhan and Hani [37] studied the water sorption kinetic of semi-refined κ-carrageenan crosslinked with glycerol and sorbitol in different concentrations. We observed in our study the same behaviors and values for the κ film as the values identified by Farhan and Hani [37] for the κ-carrageenan crosslinked with glycerol (30%) in their study.

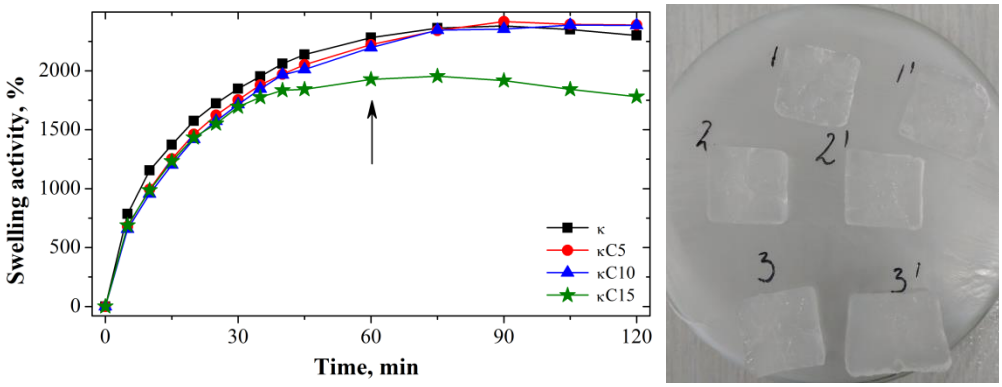

a. b.

Fig. 12. Swelling activity of the studied films in water at 25 °C for a period of 120 min (a) and the aspect of the films after 120 min in water (b)

The incorporation of the CNC nanofiller into the polymeric matrix induce a limitation of the films water absorptivity. This behavior may be attributed to the reinforcing potential of CNCs (due to their high crystallinity and surface area volume ratios) which enable good interfacial interaction and storng hydrogen bonding of the polymer matrix and CNCs, causing a modification in the structural packing of the material by restricting the chain mobility and reducing the amount of free hydroxyl groups of the matrix [22].

3.7.Dry-in time of water droplets on the surfaces and absorption

The dry-in time of a droplet depends on the RH of the surrounding environment and it is closely related to the adsorption behaviors and contact angle. The droplets dry faster if the ability of adsorption is higher and the contact angle lower.

Fig. 13 represent the test, the upper side of the figure indicating the droplets on the films immediately after dropping them, while the lower side images represent the droplets after drying. It has been observed that the droplets remained on the surface of the films, presenting a low degree of absorption and the dry-in time was of 40-45 min.

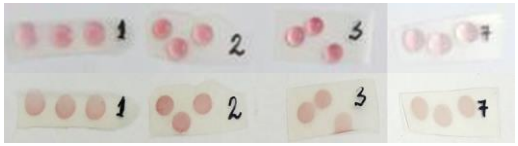

Fig. 13. The droplets on the surface of the films (κ – 7, κC5 – 1, κC10 – 2, κC15 – 3)

3.8.Contact angle measurements

Wetting properties of the nanocomposite films were evaluated by measuring the contact angle between the film surface and a water droplets (see Fig. 14).

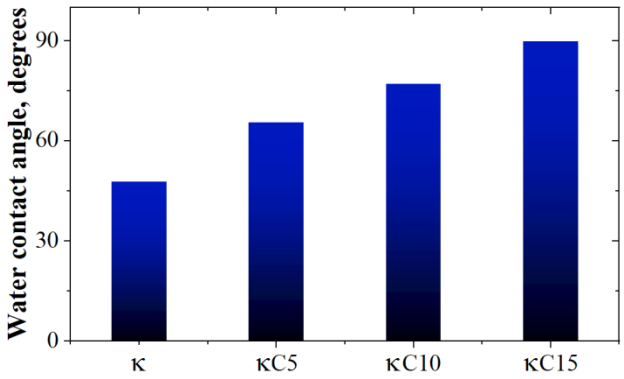

Fig. 14. Water contact angles determined for the studied films

As can be observed, the value for κ film is of 47.8° being drastically affected by the incorporation of CNCs into the polymeric matrix. The contact angle value increased with the increase of the CNCs amount, reaching a value of 89.7° for κC15 film. Even both components are considered to be hydrophilic polymers, the CNCs incorporation into the κ matrix leads to an increase of surface hydrophobicity of the composites due to the formation of strong hydrogen bonds interaction between them. They could also reduce the surface interactions between water molecules and the material and hence increasing surface hydrophobicity. These observations are in agreement with the data obtained for the other methods described above. Moreover, similar results, increase of surface hydrophobicity by CNCs incorporation into hydrophilic matrices, were reported by Zakuwan and Ahmed [22] and Abdollahi et al. [43].

It has been observed that the addition of CNCs (as nanofillers) and glycerol (as crosslinging / plasticizing agent) resulted in improved tensile strength an Young's modulus [44]. At the same time, the increase in the CNCs content "continously increased to a optimum level" being explained by Zarina and Ahmad [45] as a good dispertion of CNCs in the κ matrix. Moreover, due to CNCs properties, such as: high crystallynity and high surface area volume ratios, enables increased surface interaction between the CNC nanofiller and the κ matrix, inducing superior mechanical properties [45].

4. Conclusions

Nanocomposite formulations with different κ-carrageenan / CNC concentrations were prepared and evaluated for their structural features, interactions, and sorption properties. Infrared spectroscopy, coupled with PCA and 2DCOS indicated the presence of interactions between the two components, especially via hydrogen bonding. Moreover, X-ray diffraction indicated that the

incorporation of CNC into the κ matrix induces a certain orientation of the polymeric molecules which favour the formation of H bonds. Even though the both components are considered to be hydrophilic polymers, due to the previous mentioned interaction, the increase in the CNC content in the nanocomposite films induced a reduction in the moisture uptake as well as swelling degree, and an increase of the contact angle. At the same time, it was evidenced that water molecules link to polymer hydrophilic sites via moderate H-bonds before forming stronger H-bonds with the matrix and diffuse into the free volume of the matrix.

Acknowledgements

This work was supported by the project M-ERA.NET2 COFUND – no.73/2017 – *Eco-friendly nanoclay, nanocellulose and MIP composites for microbial formulations* – COMPIO.

References

1. M.J.M. Ridzuan, M.S. Abdul Majid, M. Afendi, S.N. Aqmariah Kanafiah, J.M. Zahri, A.G. Gibson, Characterisation of natural cellulosic fibre from *Pennisetum purpureum* stem as potential reinforcement of polymer composites, Mater. Des. 89 (2016) 839–847.
2. C.-W. Zhang, F.-Y. Li, J.-F. Li, L.-M. Wang, Q. Xie, J. Xu, S. Chen, A new biodegradable composite with open cell by combining modified starch and plant fibers, Mater. Des. 120 (2017) 222–229.
3. S. Shojaee-Aliabadi, M.A. Mohammadifar, H. Hosseini, A. Mohammadi, M. Ghasemlou, S.M. Hosseini, M. Haghshenas, R. Khaksar, Characterization of nanobiocomposite kappa-carrageenan film with *Zataria multiflora* essential oil and nanoclay, Int. J. Biol. Macromol. 69 (2014) 282–289.

4. S. Kumar, S. Raj, S. Jain, K. Chatterjee, Multifunctional biodegradable polymer nanocomposite incorporating graphene-silver hybrid for biomedical applications, Mater. Des. 108 (2016) 319–332.
5. S. Rudhziah, M.S.A. Rani, A. Ahmad, N.S. Mohamed, H. Kaddami, Potential of blend of kappa-carrageenan and cellulose derivatives for green polymer electrolyte application, Ind. Crops Prod. 72 (2015) 133–141.
6. N.R. Savadekara, V.S. Karandea, N. Vigneshwaranb, A.K. Bharimallab, S.T. Mhaske, Preparation of nano cellulose fibers and its application in kappa-carrageenan based film, Int. J. Biol. Macromol. 51 (2012) 1008–1013.
7. M.D. Sanchez-Garcia, L. Hilliou, J.M. Lagaron, Morphology and water barrier properties of nano biocomposites of k/ι-hybrid carrageenan and cellulose nanowhiskers, J. Agric. Food Chem. 58 (2010) 12847–12857.
8. L. Hilliou, F.D.S. Larotonda, P. Abreu, A.M. Ramos, A.M. Sereno, M.P. Goncalves, Effect of extraction parameters on the chemical structure and gel properties of k/i-hybrid carrageenans obtained from *Mastocarpus stellatus*, Biomol. Eng. 23 (2006) 201–208.
9. J. Kozlowska, K. Pauter, A. Sionkowska, Carrageenan-based hydrogels: Effect of sorbitol and glycerin on the stability, swelling and mechanical properties, Polym. Testing 67 (2018) 7–11.
10. B. Zhu, F. Ni, Y. Sun, X. Zhu, H. Yin, Z. Yao, Y. Du, Insight into carrageenases: major review of sources, category, property, purification method, structure, and applications, Critical Rev. Biotechnol. 38 (2018) 1261–1276.
11. T. Janjarasskul, J.M. Krochta, Edible Packaging Materials, Annual Rev. Food Sci. Technol. 1 (2010) 415–448.

12. V.K. Kotharangannagari, K. Krishnan, Biodegradable hybrid nanocomposites of starch/lysine and ZnO nanoparticles with shape memory properties, Mater. Des. 109 (2016) 590–595.
13. G. Sun, T. Liang, W. Tan, L. Wang, Rheological behaviors and physical properties of plasticized hydrogel films developed from κ-carrageenan incorporating hydroxypropyl methylcellulose, Food Hydrocolloids 85 (2018) 61–68.
14. D.M. Panaitescu, A.N. Frone, I. Chiulan, A. Casarica, C.A. Nicolae, M. Ghiurea, R. Trusca, C.M. Damian, Structural and morphological characterization of bacterial cellulose nano-reinforcements prepared by mechanical route, Mater. Des. 110 (2016) 790–801.
15. N.H. Zakaria, N. Muhammad, M.M.A.B. Abdullah, I.G. Sandu, C.L. Mei Wan, Characteristics of Thermoplastic Potato Starch/Bentonite Nanocomposite Film, IOP Conf. Series: Mater. Sci. Eng. 374 (2018) 012025.
16. I.F. Wahab, S.I. Abd Razak, Bionanocomposite film of kappa-carrageenan / nanotube clay: growth of hydroxyl apatite and model drug release, Digest J. Nanomat. Biostructures 11 (2016) 963.
17. A.A. Oun, J.-W. Rhim, Carrageenan-based hydrogels andfilms: Effect of ZnO and CuO nanoparticles on the physical, mechanical, and antimicrobial properties, Food Hydrocolloids 67 (2017) 45-53.
18. R. Venkatesan, N. Rajeswari, T.T. Thiyagu, Preparation, characterization and mechanical properties of k-Carrageenan/SiO2 nanocomposite films for antimicrobial food packaging, Bull. Mater. Sci. 40 (2017) 609–614.
19. M.A. Azizi Samir, F. Alloin, A. Dufresne, Review of recent research into cellulosic whiskers, their properties and their application in nanocomposite field, Biomacromol. 6 (2005) 612–626.

20. S. Azizi, R. Mohamad, Mechanical and barrier properties of kappacarrageenan/cellulose nanocrystals bio-nanocomposite films, IOP Conf. Series: Mater. Sci. Eng. 368 (2018) 012013.

21. Z. Kassab, F. Aziz, H. Hannache, H.B. Youcef, M. El Achaby, M. Yadava, F.-C. Chiu, Improved mechanical properties of k-carrageenan-based nanocomposite films reinforced with cellulose nanocrystals, Carbohyd. Polym. 211 (2019) 181–194.

22. S.Z. Zakuwan, I. Ahmad, Synergistic Effect of Hybridized Cellulose Nanocrystals and Organically Modified Montmorillonite on k-Carrageenan Bionanocomposites, Nanomaterials 8 (2018) 874.

23. T.B. Shalom, Y. Nevo, D. Leibler, Z. Shtein, C. Azerraf, S. Lapidot, O. Shoseyov, Cellulose Nanocrystals (CNCs) Induced Crystallization of Polyvinyl Alcohol (PVA) Super Performing Nanocomposite Films, Macromol. Biosci. 19 (2019) 1800347

24. A.M. Ili Balqis, M.A.R. Nor Khaizura, A.R. Russly, Z.A. Nur Hanania, Effects of plasticizers on the physicochemical properties of kappa-carrageenan films extracted from *Eucheuma cottonii*, Int. J. Biol. Macromol. 103 (2017) 721–732.

25. A. Bellgrove, H. Kihara, A. Iwata, M.N. Aoki, P. Heraud, Fourier transform infrared microspectroscopy as a tool to identify macroalgal propagules, J. Phycol. 45 (2009) 560–570.

26. L. Pereira, S.F. Gheda, P.J.A. Ribeiro-Claro, Analysis by Vibrational Spectroscopy of Seaweed Polysaccharides with Potential Use in Food, Pharmaceutical, and Cosmetic Industries, Int. J. Carbohyd. Chem. (2013) Article ID 537202, 7 pages.

27. C.-M. Popescu, C.M. Tibirna, I.E. Raschip, M.-C. Popescu, P. Ander, C. Vasile, Bulk and surface characterization of unbleached and bleached softwood Kraft pulp fibres, Cell. Chem. Technol. 42 (2008) 525–547.

28. M.-C. Popescu, B.-I. Dogaru, M. Goanta, D. Timpu, Structural and morphological evaluation of CNC reinforced PVA/Starch biodegradable films, Int. J. Biol. Macromol. 116 (2018) 385–393.

29. M.-C. Popescu, C. Vasile, Gh. Singurel, 2D IR correlation spectroscopy in polymer studyes, in New Trends in Natural and Synthetic Polymer Science, Eds. Zaikov G.E., Nova Science Publishers, ISBN:978-1-60021-547-6, p. 71-111, 2007

30. I. Noda, Y. Ozaki, Two-Dimensional Correlation Spectroscopy. Applications in Vibrational and Optical Spectroscopy, John Wiley & Sons, Chichester, 2004

31. C.-M. Popescu, P.T. Larsson, N. Olaru, C. Vasile, Spectroscopic study of acetylated kraft pulp fibers, Carbohyd. Polym. 88 (2012) 530–536.

32. Z. Hejri, A.A. Seifkordi, A. Ahmadpour, S.M. Zebarjad, A. Maskooki, Biodegradable starch/poly(vinyl alcohol) film reinforced with titanium dioxide nanoparticles, Int. J. Minerals Metallurgy Mater. 20 (2013) 1001.

33. K. Ichikawa, T. Mori, H. Kitano, M. Fukuda, A. Mochizuki, M. Tanaka, Fourier Transform Infrared Study on the Sorption of Water to Various Kinds of Polymer Thin Films, J. Polym. Sci. Polym. Phys. 39 (2001) 2175–2182.

34. G.K. van der Wel, O.C.G. Adan, Moisture in organic coatings – a review, Prog. Org. Coat. 37 (1999) 1–14.

35. M.-C. Popescu, B.-I. Dogaru, C.-M. Popescu, The influence of cellulose nanocrystals content on the water sorption properties of bio-based composite films, Mater. Des. 132 (2017) 170–177.

36. M.D. Torres, F. Chenlo, R. Moreira, Structural features and water sorption isotherms of carrageenans: A prediction model for hybrid carrageenans, Carbohyd. Polym. 180 (2018) 72–80.

37. A. Farhan, N.M. Hani, Characterization of edible packaging films based on semi-refined kappa-carrageenan plasticized with glycerol and sorbitol, Food Hydrocolloids 64 (2017) 48-58.

38. C. Sangwichien, G.L. Aranovich, M.D. Donohue, Density functional theory predictions of adsorption isotherms with hysteresis loops, Colloids Surf. A: Physicochem. Eng. Aspects 206 (2002) 313–320.

39. L. Guan, H. Xu, D. Huang, The investigation on states of water in different hydrophilic polymers by DSC and FTIR, J. Polym. Res. 18 (2011) 681–689.

40. M. Galizia, P. La Manna, G. Mensitieri, M. Pannico, P. Musto, Diffusion in polymers as investigated by two-dimensional correlation spectroscopy: The H2O/PCL system, J. Mol. Struct. 1069 (2014) 290–298.

41. S. Cotugno, D. Larobina, G. Mensitieri, P. Musto, G. Ragosta, A novel spectroscopic approach to investigate transport processes in polymers: the case of water-epoxy system, Polymer 42 (2001) 6431–6438.

42. Y. Jin, W. Wang, Z. Su, Spectroscopic study on water diffusion in aromatic polyamide thin film, J. Membr. Sci. 379 (2011) 121–130.

43. M. Abdollahi, M. Alboofetileh, M. Rezaei, R. Behrooz, Comparing physico-mechanical and thermal properties of alginate nanocomposite films reinforced with organic and/or inorganic nanofillers, Food Hydrocolloids 32 (2013) 416–424.

44. Z. Kassab, F. Aziz, H. Hannache, H. Ben Youcef, M. El Achaby, Improved mechanical properties of k-carrageenan-based nanocomposite films reinforced with cellulose nanocrystals, Int. J. Biol. Macromol. 123 (2019) 1248–1256.

45. S. Zarina, I. Ahmad, Biodegradsble composite films based on κ-carrageenan reinforced by cellulose nanocrystal from kenaf fibers, BioRes. 10 (2015) 256-271.